SCIENCE CHINA
Information Sciences

• RESEARCH PAPER •

October 2017, Vol. 60 102302:1–102302:16
doi: 10.1007/s11432-016-0291-9

Novel multi-tap analog self-interference cancellation architecture with shared phase-shifter for full-duplex communications

Hongtao LU, Chuan HUANG*, Shihai SHAO & Youxi TANG

National Key Laboratory of Science and Technology on Communications, University of Electronic Science and Technology of China, Chengdu 611731*, China*

Received June 14, 2016; accepted September 30, 2016; published online March 28, 2017

Abstract Multi-tap analog self-interference (SI) cancellation structures adopt parallel taps to reconstruct and then cancel SI in full-duplex radios. Each tap is usually comprised of one fixed delay line, one variable attenuator, and one optional variable phase shifter. To balance the quantity of the variable phase shifters and the achievable SI cancellation (SIC) performance, this paper proposes a novel analog SIC cancellation structure, called shared-phase-shifter constrained multi-tap structure (SMTS). In the proposed architecture, all taps share one phase shifter to emulate the dominated phase offset of the SI channel, which reduces the complexity of the implementation of the multi-tap analog SIC structure and avoids the SIC performance degradation. Then, the proposed SMTS and the existing structures are compared in terms of SIC performance and power dissipation. Finally, extensive simulations show that SMTS provides the close-to-optimal SIC performance as well as the lowest power dissipation relative to the existing multi-tap structures.

Keywords full-duplex, multi-tap structure, power dissipation, phase shifter, self-interference cancellation

Citation Lu H T, Huang C, Shao S H, et al. Novel multi-tap analog self-interference cancellation architecture with shared phase-shifter for full-duplex communications. Sci China Inf Sci, 2017, 60(10): 102302, doi: 10.1007/s11432-016-0291-9

1 Introduction

In the past years, full-duplex (FD) communications have been attracting increasing research interests [1–4]. The most challenging problem for implementing FD radios is to cancel the extremely strong self-interference (SI) from its transmitter to the local receiver. For this purpose, various analog SI cancellation (SIC) schemes have been developed [1–3], among which multi-tap analog SIC scheme was shown to achieve excellent SIC performance [1].

Existing structures of the multi-tap analog SIC, summarized in Table 1, are classified into two types: complete multi-tap structure (CMTS) and degraded multi-tap structure (DMTS). In CMTS prototyped in [5–8], each tap consisted of one fixed delay line, one variable scaler, and one variable phase shifter, as shown in Figure 1(a). The prototypes in [5] and [6] adopted 4 taps to achieve a SI reduction of 43 dB and 31 dB, respectively, where the delay lines were quasi-fixed since they were tuned manually before

* Corresponding author (email: huangch@uestc.edu.cn)

Table 1 Various multi-tap analog SIC prototypes

Paper	Type	Number of taps	BW (MHz)	SI reduction[a)] (dB)	Tuning time[b)] (ms)
Ref. [5]	CMTS	4	20	43	10
Ref. [6]	CMTS	4	30	31	–
Ref. [7]	CMTS	10	20	57	–
Ref. [8]	CMTS	4	20	35	–
Ref. [9]	DMTS	2	20	13	–
Ref. [10]	DMTS	2	10	20	0.13
Ref. [11]	DMTS	16	20	57	1
Ref. [12]	DMTS	12	20	53	–

a) The power ratio of SIs before and after the multi-tap SIC stage.

b) The required time for tuning variable scalars and variable phase shifters to maximize SIC performance.

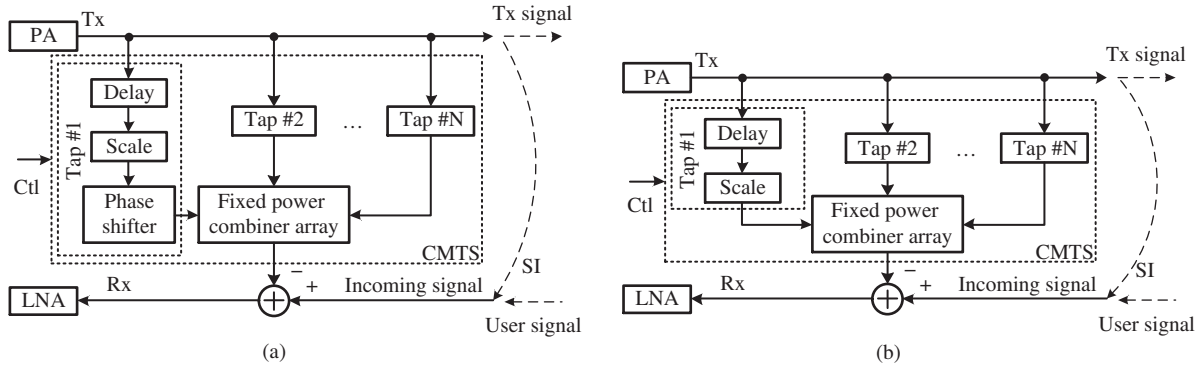

Figure 1 Multi-tap analog SIC schemes. (a) CMTS; (b) DMTS.

performing experiments and then were fixed during experiments. The prototype in [7] adopted 8 variable taps together with two quasi-fixed taps to achieve a SI reduction of 57 dB. The delays, scales, and phase shifts of the two quasi-fixed taps were tuned to cancel the strongest components of SI before performing experiments and were fixed during the execution of experiments. The prototype in [8] adopted 4 taps with a delay interval of 4 ns to achieve a SI reductions of 35 dB. To summarize, the aforementioned CMTS prototypes provided high SI reduction while the utilization of variable phase shifters increases the implementation complexity and the duration of the tuning operation.

In DMTS prototyped in [9–12], each tap consisted of a fixed delay line and a variable scaler, as shown in Figure 1(b). The prototypes in [9] and [10] reconstructed inverted versions of SI by using Qhx220[1)] and achieved a SI reduction of 13 dB and 20 dB, respectively. Since the output signal of a Qhx220 is the sum of two delayed and scaled[2)] [13] versions of its input signal, the SIC circuits of the prototypes in [9] and [10] were two-tap DMTSs. The prototype in [11] achieved a SI reduction of 48 dB with 16 taps, where the delays of the delay lines were deliberately designed to be close to the delays of the strong components of SI to achieve high SI reduction. Adopting the same way as in [11] to design the delay lines, the prototype in [12] achieved a SI reduction of 53 dB with 12 taps. To summarize, the aforementioned DMTS prototypes have simple tap circuit as well as lower SI reduction and fast convergence speed.

To balance the quantity of the variable phase shifters and the SIC performance, a novel multi-tap implement structure, called shared-phase-shifter multi-tap structure (SMTS), is proposed. The achievable SIC performance provided by SMTS is derived. In addition, this paper initially analyzes the power dissipation of SMTS as well as the power dissipation of CMTS and DMTS.

Notations. The following notations are used in this paper. Matrixes and vectors are denoted as bold

1) Quellan Inc. Qhx220 narrowband noise canceller ic. 2009.

2) The QHx220 is essentially a vector modulator[1)], which integrates an auxiliary sign inversion module to assist the integrated scalars to provide negative scales [13]. Thus, a chip of QHx220 is an enhanced two-tap DMTS rather than an elementary two-tap DMTS.

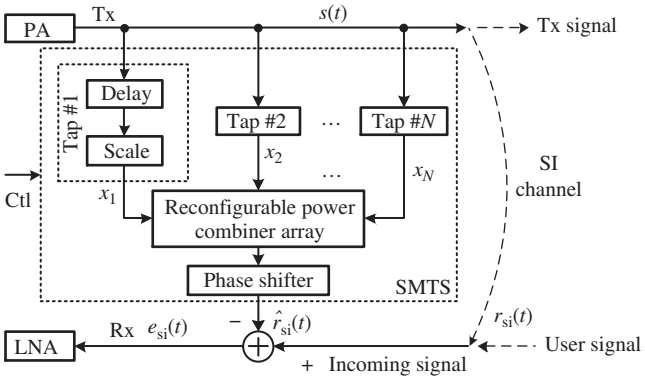

Figure 2 The proposed SMTS.

Table 2 Comparisons of CMTS, DMTS, and SMTS with N taps

Item	CMTS	DMTS	SMTS
1. Number of fixed delay lines	N	N	N
2. Number of variable scalars	N	N	N
3. Number of variable phase shifters	N	0	1
4. N-way power combiner array	1	1	1
5. Dimensions of control algorithm	$2N$	N	$N+1$

capital letters and $\boldsymbol{I}$ is the identity matrix. $(\cdot)^{\mathrm{T}}$, $(\cdot)^{\mathrm{H}}$, and $(\cdot)^*$ are the transpose, the conjugate transpose, and the complex conjugate, respectively. $\mathrm{E}\{\cdot\}$ means statistical expectation. $\mathrm{Re}\{\cdot\}$, $\mathrm{Ang}\{\cdot\}$, and $\|\cdot\|$ means the real part, phase angle, and modulus of a complex number, respectively, and j is the imaginary unit. $\mathrm{Diag}\{\boldsymbol{V}\}$ is the diagonal matrix with the same diagonal elements as a vector $\boldsymbol{V}$. $\mathrm{Sgn}\{x\}$ is a modified signum function, which returns 1 if $x \geqslant 0$ and -1 if $x < 0$. $\lceil\cdot\rceil$ is the ceiling function. $\lambda_{\min}\{\boldsymbol{F}\}$ and $\lambda_{\max}\{\boldsymbol{F}\}$ represent the minimum and maximum eigenvalues of a square matrix $\boldsymbol{F}$, respectively. $\otimes$ denotes convolution. ∇F is the gradient of function F.

2 Architecture and signal model

In this section, the architecture of the proposed SMTS is detailed. Then, the proposed SMTS is compared with CMTS and DMTS in terms of architecture. Finally, the signals in SMTS are modeled.

2.1 Architecture

Figure 2 shows the considered FD radio frontend, where the transmit signal couples into the receiver via the SI channel and causes strong SI before the low-noise amplifier (LNA). To cancel this strong SI, the proposed SMTS creates an estimated SI with N replicas of the transmit signal, and then subtracts it from the incoming signal, where N is the number of taps.

In the proposed SMTS, each tap has an input signal coupled from the transmitter, which is essentially a replica of the transmit signal, and is delayed by a fixed delay line and scaled by a variable scaler. Then, all the delayed-and-scaled signals are summed up in a proposed reconfigurable power combiner array, which feeds the sum signal to a shared phase shifter to align with the phase of the SI. Finally, the reconstructed SI is yielded by the shared phase shifter and then subtracted from the incoming signal by a power combiner. Since the transmitter and receiver are in close proximity, the SI channel contains leakage path which is far stronger than the rest components, and thus is close to a flat fading channel (The Ricean K-factor of a practical SI channel may be up to 22 dB [14]). Thus the key point of SMTS is to use the shared phase shifter to emulate the dominated phase offset of the SI channel, to which the SIC performance is highly sensitive [15].

Architecture comparisons between SMTS, CMTS and DMTS are summarized in Table 2. Relative to CMTS, SMTS saves $N-1$ variable phase shifters and degrades the control algorithm by $N-1$ dimensions. Relative to DMTS, SMTS adopts only an additional variable phase shifter and upgrades the control algorithm by only 1 dimension.

The drawbacks of DMTS are summarized as follows:

(i) The variable scalers are implemented by either variable attenuators or variable amplifiers all of which only can implement nonnegative scales [16]. Thus, performance degradation of this scheme will occur if part of the implemented scales are negative. In SMTS, if all scales are negative, the common factor -1 among the scales can be implemented by the shared phase shifter since -1 is equivalent to a phase offset of π, which will be invalid if only part of the scales are negative. Thus, the nonnegative constraint for scales exists in SMTS. To depose this nonnegative constraint, a reconfigurable power combiner array is developed in this paper.

(ii) The misalignment of phase between the reconstructed and the incoming SI may cause significant degradation of the SIC performance [15]. This phase-misalignment is difficult to be compensated for DMTS since no phase shifter is adopted. Thus, the SIC performance provided by DMTS is degraded significantly. In SMTS, the shared phase shifter compensates the dominated phase difference between the reconstructed and the incoming SI to mitigate the performance degradation caused by it.

The drawbacks of CMTS are summarized as follows:

(i) CMTS achieves high SIC performance at the cost of potential high power dissipation. The reason is detailed qualitatively here and the demonstration will be given in Subsection 4.1. The reason is that, in the N-way power combiner array, the power of the output signal may be far smaller than the power sum of the N input signals due to the correlations among the N input signals. In SMTS, the correlations among the input signals of the power combiner array are weak, since they are not shifted in phase and then have relatively large phase-misalignment among them. Thus, SMTS potentially has a lower power dissipation than CMTS.

(ii) CMTS adopts N variable scalers and N variable phase shifters, and thus requires a $2N$-dimension tuning algorithm, which is complicated for implements and has too slow convergence speed to track time-variant SI channels. Adopting one shared phase shifter along with N scalars, SMTS only requires an $(N+1)$-dimension tuning algorithm.

2.2 Signal model

This paper mainly focuses on the SIC, and thus the thermal noise and the remote user signal are omitted for the signal model in the sequel. The transmit signal is modeled as [17]

$$s(t) = \mathrm{Re}\{b(t)\exp(\mathrm{j}\omega_c t)\}, \tag{1}$$

where $b(t)$ is the complex lowpass equivalent, ω_c is the radian carrier frequency, and j is the imaginary unit.

The transmit signal $s(t)$ propagates to the front of the local receiver via the SI channel, which is usually modeled as a multipath channel. Then, strong SI signal at the front of the receiver is given as

$$r_{\mathrm{si}}(t) = \sum_{m=1}^{M} h_m \mathrm{Re}\{b(t-d_m)\exp(\mathrm{j}\omega_c(t-d_m)+\mathrm{j}\varphi_m)\} = \mathrm{Re}\{\boldsymbol{D}_{\mathrm{si}}^{\mathrm{T}}\boldsymbol{Q}\boldsymbol{H}\exp(\mathrm{j}\omega_c t)\}, \tag{2}$$

where m, d_m, h_m, and φ_m are the index, delay, scale, and phase shift of mth path, respectively, M is the path number, $\boldsymbol{D}_{\mathrm{si}} = [b(t-d_1), b(t-d_2), \ldots, b(t-d_M)]^{\mathrm{T}}$, $\boldsymbol{Q} = \mathrm{Diag}([\exp(-\mathrm{j}\omega_c d_1), \exp(-\mathrm{j}\omega_c d_2), \ldots, \exp(-\mathrm{j}\omega_c d_M)])$, and $\boldsymbol{H} = [h_1\exp(\mathrm{j}\varphi_1), h_2\exp(\mathrm{j}\varphi_2), \ldots, h_M\exp(\mathrm{j}\varphi_M)]^{\mathrm{T}}$.

In the SMTS circuit shown in Figure 2, nth tap delays and scales a coupled replica of the transmit signal $s(t)$ and yields an adjusted signal x_n. Being the phase-shifted version of the sum of $\{x_1, x_2, \ldots, x_N\}$, the reconstructed SI yielded by the proposed SMTS is expressed as

$$\hat{r}_{\mathrm{si}}(t) = \sum_{n=1}^{N} a_n \mathrm{Re}\{b(t-\tau_n)\exp(\mathrm{j}\omega_c(t-\tau_n)+\mathrm{j}\phi)\} = \mathrm{Re}\{\boldsymbol{D}_{\mathrm{rc}}^{\mathrm{T}}\boldsymbol{O}\boldsymbol{A}\exp(\mathrm{j}\omega_c t)\}, \tag{3}$$

where n, a_n, and τ_n are the index, scale, and delay of nth tap, respectively, $\boldsymbol{D}_{\rm rc} = [b(t-\tau_1), b(t-\tau_2), \ldots, b(t-\tau_N)]^{\rm T}$, $\boldsymbol{O} = {\rm Diag}([\exp(-{\rm j}\omega_c\tau_1), \exp(-{\rm j}\omega_c\tau_2), \ldots, \exp(-{\rm j}\omega_c\tau_N)])$, $\boldsymbol{A} = \exp({\rm j}\phi)[a_1, a_2, \ldots, a_N]^{\rm T}$ is the adjustable tap coefficient vector, and ϕ is the phase offset of the shared phase shifter. The aforementioned nonnegative constraint shows that $a_i \geqslant 0$ is satisfied for $i = 1, 2, \ldots, N$. Besides, τ_1, $\tau_2, \ldots, \tau_N$ are different from one another, since the taps which have the same delays can be combined and considered as a single tap.

Subtracting the reconstructed SI $\hat{r}_{\rm si}(t)$ from the received SI $r_{\rm si}(t)$, the residual SI is given as

$$e_{\rm si}(t) = {\rm Re}\{(\boldsymbol{D}_{\rm si}^{\rm T}\boldsymbol{Q}\boldsymbol{H} - \boldsymbol{D}_{\rm rc}^{\rm T}\boldsymbol{O}\boldsymbol{A})\exp({\rm j}\omega_c t)\}. \tag{4}$$

The power of $e_{\rm si}(t)$ is computed as

$$P_{\rm e} = {\rm E}\{\|e_{\rm si}(t)\|^2\} = P_{\rm tx}(I_{\rm t/r} - 2{\rm Re}\{\boldsymbol{H}^{\rm H}\boldsymbol{Q}^{\rm H}\boldsymbol{C}_b^{\rm H}\boldsymbol{O}\boldsymbol{A}\} + \boldsymbol{A}^{\rm H}\boldsymbol{O}^{\rm H}\boldsymbol{R}_b\boldsymbol{O}\boldsymbol{A}), \tag{5}$$

where $I_{\rm t/r} = {\rm E}\{\|\boldsymbol{D}_{\rm si}^{\rm T}\boldsymbol{Q}\boldsymbol{H}\|^2\}/{\rm E}\{\|b(t)\|^2\} = {\rm E}\{\|r_{\rm si}(t)\|^2\}/P_{\rm tx}$ is the power gain of the SI channel, $\boldsymbol{R}_b$ is the normalized auto-correlation matrix of $\boldsymbol{D}_{\rm rc}$ and given by

$$\boldsymbol{R}_b = \begin{bmatrix} 1 & R_b(\tau_1-\tau_2) & \cdots & R_b(\tau_1-\tau_N) \\ R_b(\tau_2-\tau_1) & 1 & \cdots & R_b(\tau_2-\tau_N) \\ \vdots & \vdots & \ddots & \vdots \\ R_b(\tau_N-\tau_1) & R_b(\tau_N-\tau_2) & \cdots & 1 \end{bmatrix},$$

$\boldsymbol{C}_b$ is the normalized cross-correlation matrix of $\boldsymbol{D}_{\rm rc}$ and $\boldsymbol{D}_{\rm si}$ and given by

$$\boldsymbol{C}_b = \begin{bmatrix} R_b(\tau_1-d_1) & R_b(\tau_1-d_2) & \cdots & R_b(\tau_1-d_M) \\ R_b(\tau_2-d_1) & R_b(\tau_2-d_2) & \cdots & R_b(\tau_2-d_M) \\ \vdots & \vdots & \ddots & \vdots \\ R_b(\tau_N-d_1) & R_b(\tau_N-d_2) & \cdots & R_b(\tau_N-d_M) \end{bmatrix},$$

$R_b(\tau)$ is the normalized auto-correlation function of $b(t)$, and $P_{\rm tx}$ is the constant transmit power.

3 SIC performance

This section aims to analyzing the SIC performance provided by SMTS. First, the reconfigurable power combiner array is detailed to depose the nonnegative constraint on the scalars in SMTS. Next, an iteration algorithm is developed to minimize the power of the residual SI $P_{\rm e}$ in the field of real numbers instead of the field of nonnegative real numbers. Then, the SI cancellation performance provided by SMTS is derived. Finally, SMTS is compared with CMTS and DMTS in terms of SI cancellation performance.

3.1 Reconfigurable power combiner array

For SMTS, $\boldsymbol{A}$ can be rewritten as $\boldsymbol{A} = \tilde{\boldsymbol{A}}\exp({\rm j}\phi)$, where $\tilde{\boldsymbol{A}} = [a_1, a_2, \ldots, a_N]^{\rm T}$ is the scale vector. Existing scalar devices only can implement the magnitude of the elements of $\tilde{\boldsymbol{A}}$, and thus this subsection develops a reconfigurable power combiner array to implement the signum of the elements of $\tilde{\boldsymbol{A}}$ along with the function of an N-way power combiner array. In the sequel, the number of taps N is assumed to be an integer power of 2 for simplicity. If N is not a power of 2, $2^{\lceil \log_2(N) \rceil} - N$ zeros need to be padded.

Figure 3 illustrates the reconfigurable power combiner array, which is a "tree" of the sum-diff-circuits (SuDiCs). Each SuDiC, observed from Figure 3(a), consists of one rat-race coupler cascaded by one selector. The selector strobes the outputs of the rat-race coupler alternatively. The scattering matrix of

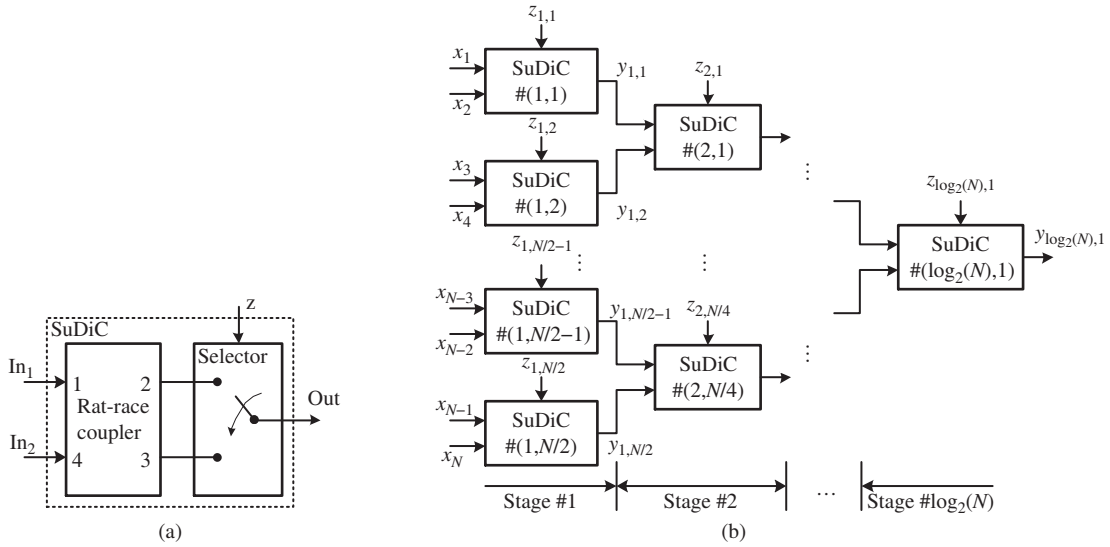

Figure 3 Design of the reconfigurable power combiner array. (a) Structure of a SuDiC; (b) structure of the proposed reconfigurable power combiner array, where x_i represents the signal from the ith tap.

the rat-race coupler is given in [18] and expressed as

$$\frac{-\mathrm{j}}{\sqrt{2}}\begin{bmatrix}0 & 1 & 1 & 0\\ 1 & 0 & 0 & -1\\ 1 & 0 & 0 & 1\\ 0 & -1 & 1 & 0\end{bmatrix},$$

and then the scattering matrix of the SuDiC shown in Figure 3(a) is computed as $-\mathrm{j}\,[1,\ (-1)^z]/\sqrt{2}$, where z is the switch signal of the selector. If $z=1$, the 2nd port of the rat-race coupler is connected to the output port of the SuDiC. If $z=0$, the 3rd port of the rat-race coupler is connected to the output port of the SuDiC.

The reconfigurable power combiner array has a tree structure and is shown in Figure 3(b), where x_n is the nth input signal of the reconfigurable power combiner array, i.e., the adjusted replica of the transmit signal in the nth tap, and given as $x_n = \|a_n\|\mathrm{Re}\{b(t-\tau_n)\exp(\mathrm{j}\omega_c(t-\tau_n)+\mathrm{j}\phi_n)\}$. The computational method for the switch signal at the selector in the kth SuDiC of the ith stage is given as

$$z_{i,k} = \begin{cases} 0, & \text{if } \mathrm{Sgn}\{a_{(k-1)\times 2^i+1}\} = \mathrm{Sgn}\{a_{(k-1)\times 2^i+2^{i-1}+1}\},\\ 1, & \text{otherwise,}\end{cases} \tag{6}$$

where $i = 1, 2, \ldots, \log_2(N)$ and $k = 1, 2, \ldots, N/2^i$. The final output of the reconfigurable power combiner array $y_{\log_2(N),1}$ is derived below by mathematical induction.

Basis: The output of the kth SuDiC at the first stage can be computed as

$$y_{1,k} = \left(\frac{-\mathrm{j}}{\sqrt{2}}\right)^1 \mathrm{Sgn}\{a_{2^1(k-1)+1}\} \sum_{n=2^1(k-1)+1}^{2^1 k} a_n \mathrm{Re}\{b(t-\tau_n)\exp(\mathrm{j}\omega_c(t-\tau_n)+\mathrm{j}\phi_n)\}. \tag{7}$$

Inductive step: Assuming

$$y_{i-1,2m-1} = \left(-\mathrm{j}/\sqrt{2}\right)^{i-1} \mathrm{Sgn}\{a_{2^{i-1}(2m-2)+1}\} \sum_{n=2^{i-1}(2m-2)+1}^{2^{i-1}(2m-1)} a_n \mathrm{Re}\{b(t-\tau_n)\exp(\mathrm{j}\omega_c(t-\tau_n)+\mathrm{j}\phi_n)\}$$

and

$$y_{i-1,2m} = \left(-\mathrm{j}/\sqrt{2}\right)^{i-1} \mathrm{Sgn}\{a_{2^{i-1}(2m-1)+1}\} \sum_{n=2^{i-1}(2m-1)+1}^{2^{i-1}2m} a_n \mathrm{Re}\{b(t-\tau_n)\exp(\mathrm{j}\omega_c(t-\tau_n)+\mathrm{j}\phi_n)\},$$

the output signal of SuDiC#(i,k) is computed as

$$\begin{aligned} y_{i,m} &= -\mathrm{j}(y_{i-1,2m-1}+(-1)^{z_{i,m}}y_{i-1,2m})/\sqrt{2} \\ &= \left(\frac{-\mathrm{j}}{\sqrt{2}}\right)^{i}\mathrm{Sgn}\{a_{2^{i-1}(2m-2)+1}\}\sum_{n=2^{i-1}(2m-2)+1}^{2^{i-1}(2m-1)}a_n\mathrm{Re}\{b(t-\tau_n)\exp(\mathrm{j}\omega_c(t-\tau_n)+\mathrm{j}\phi_n)\} \\ &\quad+\left(\frac{-\mathrm{j}}{\sqrt{2}}\right)^{z_{i,m}}(-\mathrm{j})^{i}\mathrm{Sgn}\{a_{2^{i-1}(2m-1)+1}\}\sum_{n=2^{i-1}(2m-1)+1}^{2^{i-1}2m}a_n\mathrm{Re}\{b(t-\tau_n)\exp(\mathrm{j}\omega_c(t-\tau_n)+\mathrm{j}\phi_n)\} \\ &= \left(\frac{-\mathrm{j}}{\sqrt{2}}\right)^{i}\mathrm{Sgn}\{a_{2^{i}(m-1)+1}\}\sum_{n=2^{i}(m-1)+1}^{2^{i}m}a_n\mathrm{Re}\{b(t-\tau_n)\exp(\mathrm{j}\omega_c(t-\tau_n)+\mathrm{j}\phi_n)\}, \end{aligned} \tag{8}$$

where $z_{i,m}$ is obtained by (6).

Eq. (8) is satisfied by the output signal of any SuDiC in the reconfigurable power combiner array. Substituting $i=\log_2(N)$ and $m=1$ into (8) yields the final output of the reconfigurable power combiner array, given as

$$y_{\log_2(N),1}=\left(-\mathrm{j}/\sqrt{2}\right)^{\log_2(N)}\mathrm{Sgn}(a_1)\sum_{n=1}^{N}a_n\mathrm{Re}\{b(t-\tau_n)\exp(\mathrm{j}\omega_c(t-\tau_n)+\mathrm{j}\phi_n)\}. \tag{9}$$

The relationship between $\hat{r}_{\mathrm{si}}(t)$ in (3) and $y_{\log_2(N),1}$ is given as $y_{\log_2(N),1}=(-\mathrm{j})^{\log_2(N)}\mathrm{Sgn}(a_1)\hat{r}_{\mathrm{si}}(t)/\sqrt{N}$, which is an attenuated and shifted-in-phase version of the desired $\hat{r}_{\mathrm{si}}(t)$. $(-\mathrm{j})^{\log_2(N)}\mathrm{Sgn}(a_1)$ is the phase offset and can be compensated by the shared phase shifter. $\sqrt{N}$ is the insertion loss of the reconfigurable power combiner array, which is equal to $2^{\lceil\log_2(N)\rceil/2}$ if N is not an integer power of 2, and can be compensated by the scalars.

Proposition 1. The application of $\tilde{\boldsymbol{A}}$ is comprised of three steps: (1) Configure the scalars with $2^{\lceil\log_2(N)\rceil/2}[\|a_1\|,\|a_2\|,\ldots,\|a_N\|]^{\mathrm{T}}$. (2) Substitute $\{a_1,a_2,\ldots,a_N\}$ into (6) to generate the switch signals of the selectors in the reconfigurable power combiner array. (3) Increase the phase offset of the shared phase shifter by $\mathrm{Ang}\{\mathrm{Sgn}(a_1)(\mathrm{j})^{\log_2(N)}\}$.

3.2 Algorithm

To derive the maximum SIC performance provided by SMTS, the power of the residual SI P_{e} given in (5) has to be minimized. To minimize P_{e} in (5), the optimal adjustable tap coefficient vector $\boldsymbol{A}$ can be obtained by jointly optimizing $\tilde{\boldsymbol{A}}$ and ϕ. The optimal $\tilde{\boldsymbol{A}}$ and ϕ to minimize P_{e} must satisfy $\nabla P_{\mathrm{e}}=0$ [19] and $\mathrm{Re}\{\boldsymbol{H}^{\mathrm{H}}\boldsymbol{Q}^{\mathrm{H}}\boldsymbol{C}_b^{\mathrm{H}}\boldsymbol{O}\tilde{\boldsymbol{A}}\exp(\mathrm{j}\phi)\}\geqslant 0$, which are derived as

$$\begin{cases}\tilde{\boldsymbol{A}}=\mathrm{Re}\{\boldsymbol{O}^{\mathrm{H}}\boldsymbol{R}_b\boldsymbol{O}\}^{-1}\mathrm{Re}\{\boldsymbol{O}^{\mathrm{H}}\boldsymbol{C}_b\boldsymbol{Q}\boldsymbol{H}\exp(-\mathrm{j}\phi)\},\\ \phi=\mathrm{Ang}\{\boldsymbol{H}^{\mathrm{T}}\boldsymbol{Q}^{\mathrm{T}}\boldsymbol{C}_b^{\mathrm{T}}\boldsymbol{O}^{*}\tilde{\boldsymbol{A}}\}.\end{cases} \tag{10}$$

In the following, an algorithm is developed to solve (10) for the real number case, since the nonnegative constraint on the elements of $\tilde{\boldsymbol{A}}$ can be deposed by the reconfigurable power combiner array. The algorithm is based on iteration operations and a subscript k is add to $\tilde{\boldsymbol{A}}$, ϕ, and P_{e} to identify their values after the kth iteration. The numerical algorithm is detailed in the sequel.

Priori knowledge. In the initial state, i.e., the 0th iteration, $\phi_0=0$, $\tilde{\boldsymbol{A}}_0=0$, and $P_{\mathrm{e}}(0)=P_{\mathrm{tx}}I_{\mathrm{t/r}}$. In the kth iteration, $\tilde{\boldsymbol{A}}_{k-1}$ and ϕ_{k-1} are already known, and $\tilde{\boldsymbol{A}}_k$ and ϕ_k are computed with the following two steps.

Step 1. Applying the shared phase shifter with ϕ_{k-1} and tuning the N scalers to minimize the power of the residual SI, the optimal scales can be computed with (10) and given as $\tilde{\boldsymbol{A}}_k=\mathrm{Re}\{\boldsymbol{O}^{\mathrm{H}}\boldsymbol{R}_b\boldsymbol{O}\}^{-1}\mathrm{Re}\{\boldsymbol{O}^{\mathrm{H}}\boldsymbol{C}_b\boldsymbol{Q}\boldsymbol{H}\exp(-\mathrm{j}\phi_{k-1})\}$. The power of the corresponding residual SI is computed as

$$P_{\mathrm{e}}(k-1\to k)=P_{\mathrm{tx}}(I_{\mathrm{t/r}}-\mathrm{Re}\{\boldsymbol{O}^{\mathrm{H}}\boldsymbol{C}_b\boldsymbol{Q}\boldsymbol{H}\exp(-\mathrm{j}\phi_{k-1})\}^{\mathrm{T}}\mathrm{Re}\{\boldsymbol{O}^{\mathrm{H}}\boldsymbol{R}_b\boldsymbol{O}\}^{-1}\mathrm{Re}\{\boldsymbol{O}^{\mathrm{H}}\boldsymbol{C}_b\boldsymbol{Q}\boldsymbol{H}\exp(-\mathrm{j}\phi_{k-1})\}).$$

Step 2. Configuring $\tilde{\boldsymbol{A}}_k$ by following Proposition 1 and tuning the shared phase shifter to minimize the power of the residual SI, the optimal phase offset can be computed with (10) and given as $\phi_k = \mathrm{Ang}\{\boldsymbol{O}^{\mathrm{H}}\boldsymbol{C}_b\boldsymbol{Q}\boldsymbol{H}^{\mathrm{T}}\tilde{\boldsymbol{A}}_k\}$. The power of the corresponding residual SI is computed as

$$\begin{aligned}P_{\mathrm{e}}(k) = P_{\mathrm{tx}}\big(&I_{\mathrm{t/r}} - 2\|\mathrm{Re}\{\boldsymbol{O}^{\mathrm{H}}\boldsymbol{C}_b\boldsymbol{Q}\boldsymbol{H}\exp(-\mathrm{j}\phi_{k-1})\}^{\mathrm{T}}\mathrm{Re}\{\boldsymbol{O}^{\mathrm{H}}\boldsymbol{R}_b\boldsymbol{O}\}^{-1}\boldsymbol{O}^{\mathrm{H}}\boldsymbol{C}_b\boldsymbol{Q}\boldsymbol{H}\| \\ &+ \mathrm{Re}\{\boldsymbol{O}^{\mathrm{H}}\boldsymbol{C}_b\boldsymbol{Q}\boldsymbol{H}\exp(-\mathrm{j}\phi_{k-1})\}^{\mathrm{T}}\mathrm{Re}\{\boldsymbol{O}^{\mathrm{H}}\boldsymbol{R}_b\boldsymbol{O}\}^{-1}\mathrm{Re}\{\boldsymbol{O}^{\mathrm{H}}\boldsymbol{C}_b\boldsymbol{Q}\boldsymbol{H}\exp(-\mathrm{j}\phi_{k-1})\}\big).\end{aligned}$$

Deriving

$$\begin{aligned}P_{\mathrm{e}}(k-1) - P_{\mathrm{e}}(k-1\to k) = {}& P_{\mathrm{tx}}\mathrm{Re}\{\boldsymbol{O}^{\mathrm{H}}\boldsymbol{C}_b\boldsymbol{Q}\boldsymbol{H}(\exp(-\mathrm{j}\phi_{k-1}) - \exp(-\mathrm{j}\phi_{k-2}))\}^{\mathrm{T}}\mathrm{Re}\{\boldsymbol{O}^{\mathrm{H}}\boldsymbol{R}_b\boldsymbol{O}\}^{-1} \\ &\times \mathrm{Re}\{\boldsymbol{O}^{\mathrm{H}}\boldsymbol{C}_b\boldsymbol{Q}\boldsymbol{H}(\exp(-\mathrm{j}\phi_{k-1}) - \exp(-\mathrm{j}\phi_{k-2}))\} \geqslant 0\end{aligned}$$

and

$$\begin{aligned}&P_{\mathrm{e}}(k-1\to k) - P_{\mathrm{e}}(k) \\ &\quad= 2P_{\mathrm{tx}}(\|\mathrm{Re}\{\boldsymbol{O}^{\mathrm{H}}\boldsymbol{C}_b\boldsymbol{Q}\boldsymbol{H}\exp(-\mathrm{j}\phi_{k-1})\}^{\mathrm{T}}\mathrm{Re}\{\boldsymbol{O}^{\mathrm{H}}\boldsymbol{R}_b\boldsymbol{O}\}^{-1}\boldsymbol{O}^{\mathrm{H}}\boldsymbol{C}_b\boldsymbol{Q}\boldsymbol{H}\exp(-\mathrm{j}\phi_{k-1})\| \\ &\qquad- \mathrm{Re}\{\mathrm{Re}\{\boldsymbol{O}^{\mathrm{H}}\boldsymbol{C}_b\boldsymbol{Q}\boldsymbol{H}\exp(-\mathrm{j}\phi_{k-1})\}^{\mathrm{T}}\mathrm{Re}\{\boldsymbol{O}^{\mathrm{H}}\boldsymbol{R}_b\boldsymbol{O}\}^{-1}\boldsymbol{O}^{\mathrm{H}}\boldsymbol{C}_b\boldsymbol{Q}\boldsymbol{H}\exp(-\mathrm{j}\phi_{k-1})\}) \\ &\quad\geqslant 0\end{aligned}$$

yields $P_{\mathrm{e}}(k-1) \geqslant P_{\mathrm{e}}(k-1\to k) \geqslant P_{\mathrm{e}}(k)$. That is to say the power of the residual SI is reduced from $P_{\mathrm{e}}(k-1)$ down to $P_{\mathrm{e}}(k)$ by updating the tap coefficient vector from $\tilde{\boldsymbol{A}}_{k-1}\exp(\mathrm{j}\phi_{k-1})$ to $\tilde{\boldsymbol{A}}_k\exp(\mathrm{j}\phi_k)$. Executing the two steps alternately by k times yields a sequence $P_{\mathrm{e}}(0)\,P_{\mathrm{e}}(1)\,\cdots\,P_{\mathrm{e}}(k)$, which is a monotonically decreasing nonnegative sequence and thus will converge as k increases. Therefore, $\tilde{\boldsymbol{A}}_\infty$ and ϕ_∞ are the solutions of (10) and $P_{\mathrm{e}}(\infty)$ is the minimum power of the residual SI in SMTS. In a word,

Proposition 2. Executing $\tilde{\boldsymbol{A}} = \mathrm{Re}\{\boldsymbol{O}^{\mathrm{H}}\boldsymbol{R}_b\boldsymbol{O}\}^{-1}\mathrm{Re}\{\boldsymbol{O}^{\mathrm{H}}\boldsymbol{C}_b\boldsymbol{Q}\boldsymbol{H}\exp(-\mathrm{j}\phi)\}$ and $\phi = \mathrm{Ang}\{\boldsymbol{H}^{\mathrm{T}}\boldsymbol{Q}^{\mathrm{T}}\boldsymbol{C}_b^{\mathrm{T}}\boldsymbol{O}^*\tilde{\boldsymbol{A}}\}$ alternatively yields the solutions of (10).

The developed numerical algorithm is shown in Algorithm 1 in form of pseudo-codes, where the fourth line and the fifth line correspond to Step 1 and Step 2, respectively.

Algorithm 1 The numerical algorithm to solve (10)

Require: Given threshold P_{th}, one temporary variable k;
1: $\tilde{\boldsymbol{A}}_0 \Leftarrow 0$, $P_{\mathrm{e}}(0) \Leftarrow P_{\mathrm{tx}}I_{\mathrm{t/r}}$, $\phi_0 \Leftarrow 0$, $k \Leftarrow 0$;
2: **repeat**
3: $\quad k \Leftarrow k+1$;
4: $\quad \tilde{\boldsymbol{A}}_k \Leftarrow \mathrm{Re}\{\boldsymbol{O}^{\mathrm{H}}\boldsymbol{R}_b\boldsymbol{O}\}^{-1}\mathrm{Re}\{\boldsymbol{O}^{\mathrm{H}}\boldsymbol{C}_b\boldsymbol{Q}\boldsymbol{H}\exp(-\mathrm{j}\phi_{k-1})\}$;
5: $\quad \phi_k \Leftarrow \mathrm{Ang}\{\boldsymbol{O}^{\mathrm{H}}\boldsymbol{C}_b\boldsymbol{Q}\boldsymbol{H}^{\mathrm{T}}\tilde{\boldsymbol{A}}_k\}$;
6: $\quad P_{\mathrm{e}}(k) \Leftarrow P_{\mathrm{tx}}(I_{\mathrm{t/r}} - \mathrm{Re}\{\boldsymbol{H}^{\mathrm{H}}\boldsymbol{Q}^{\mathrm{H}}\boldsymbol{C}_b^{\mathrm{H}}\boldsymbol{O}\tilde{\boldsymbol{A}}_k\exp(\mathrm{j}\phi_k)\} + \tilde{\boldsymbol{A}}_k^{\mathrm{T}}\boldsymbol{O}^{\mathrm{H}}\boldsymbol{R}_b\boldsymbol{O}\tilde{\boldsymbol{A}}_k)$;
7: **until** $\|P_{\mathrm{e}}(k) - P_{\mathrm{e}}(k-1)\| \leqslant P_{\mathrm{th}}$

3.3 SIC performance

This subsection derives the expression of the SIC performance provided by SMTS. First, the SIC performance for a generalized multi-tap SIC circuit is defined as the power ratio of the strong SI before this multi-tap SIC circuit to the residual SI after this multi-tap SIC circuit, expressed as

$$G = \mathrm{E}\{\|r_{\mathrm{si}}(t)\|^2\}/P_{\mathrm{e}} = I_{\mathrm{t/r}}(I_{\mathrm{t/r}} - 2\mathrm{Re}\{\boldsymbol{H}^{\mathrm{H}}\boldsymbol{Q}^{\mathrm{H}}\boldsymbol{C}_b^{\mathrm{H}}\boldsymbol{O}\boldsymbol{A}\} + \boldsymbol{A}^{\mathrm{H}}\boldsymbol{O}^{\mathrm{H}}\boldsymbol{R}_b\boldsymbol{O}\boldsymbol{A})^{-1}, \tag{11}$$

where P_{e} is obtained from (5).

After the numerical algorithm developed in last subsection converges, the optimal tap coefficient vector to minimize the power of the residual SI in SMTS is expressed as $\boldsymbol{A}_{\mathrm{SMTS}} = \tilde{\boldsymbol{A}}_\infty\exp(\mathrm{j}\phi_\infty) = \mathrm{Re}\{\boldsymbol{O}^{\mathrm{H}}\boldsymbol{R}_b\boldsymbol{O}\}^{-1}\mathrm{Re}\{\boldsymbol{O}^{\mathrm{H}}\boldsymbol{C}_b\boldsymbol{Q}\boldsymbol{H}\exp(-\mathrm{j}\phi_\infty)\}\exp(\mathrm{j}\phi_\infty)$, and the minimized power of the residual SI is expressed as $P_{\mathrm{e}}(\infty) = P_{\mathrm{tx}}\big(I_{\mathrm{t/r}} - \mathrm{Re}\{\boldsymbol{O}^{\mathrm{H}}\boldsymbol{C}_b\boldsymbol{Q}\boldsymbol{H}\exp(-\mathrm{j}\phi_\infty)\}^{\mathrm{T}}\mathrm{Re}\{\boldsymbol{O}^{\mathrm{H}}\boldsymbol{R}_b\boldsymbol{O}\}^{-1}\mathrm{Re}\{\boldsymbol{O}^{\mathrm{H}}\boldsymbol{C}_b\boldsymbol{Q}\boldsymbol{H}\exp(-\mathrm{j}\phi_\infty)\}\big)$. Substituting $\boldsymbol{A}_{\mathrm{SMTS}}$ into (11) yields the SIC performance provided by SMTS, given as

$$G_{\mathrm{SMTS}} = I_{\mathrm{t/r}}(I_{\mathrm{t/r}} - \mathrm{Re}\{\boldsymbol{O}^{\mathrm{H}}\boldsymbol{C}_b\boldsymbol{Q}\boldsymbol{H}\exp(-\mathrm{j}\phi_\infty)\}^{\mathrm{T}}\mathrm{Re}\{\boldsymbol{O}^{\mathrm{H}}\boldsymbol{R}_b\boldsymbol{O}\}^{-1}\mathrm{Re}\{\boldsymbol{O}^{\mathrm{H}}\boldsymbol{C}_b\boldsymbol{Q}\boldsymbol{H}\exp(-\mathrm{j}\phi_\infty)\})^{-1}. \tag{12}$$

In (12), only $\boldsymbol{C}_b$ and $\boldsymbol{R}_b$ are devisable at the system design stage and can be designed by changing the number and delay of the delay lines. That is to say

Proposition 3. The number and delay of the delay lines are the most important factors for the design of SMTS to achieve high SIC performance in SMTS.

3.4 SIC performance comparison

This subsection compares SMTS with CMTS and DMTS in terms of SIC performance. The SIC performance provided by CMTS is derived in Appendix A and denoted by G_{CMTS}. To compare G_{CMTS} and G_{SMTS}, $1/G_{\mathrm{SMTS}}-1/G_{\mathrm{CMTS}}=(\boldsymbol{A}_{\mathrm{SMTS}}-\boldsymbol{O}^{-1}\boldsymbol{R}_b^{-1}\boldsymbol{C}_b\boldsymbol{Q}\boldsymbol{H})^{\mathrm{H}}\boldsymbol{O}^{\mathrm{H}}\boldsymbol{R}_b\boldsymbol{O}(\boldsymbol{A}_{\mathrm{SMTS}}-\boldsymbol{O}^{-1}\boldsymbol{R}_b^{-1}\boldsymbol{C}_b\boldsymbol{Q}\boldsymbol{H})/I_{\mathrm{t/r}}\geqslant 0$ is derived, and then we have $G_{\mathrm{SMTS}}\leqslant G_{\mathrm{CMTS}}$, i.e., SMTS cannot provide a higher SIC performance than CMTS. The SIC performance provided by DMTS, derived in Appendix B and denoted by G_{DMTS}, has a upper bound $\hat{G}_{\mathrm{DMTS}}$, i.e., $G_{\mathrm{DMTS}}\leqslant\hat{G}_{\mathrm{DMTS}}$. The discussions in Subsection 3.2 show that $\hat{G}_{\mathrm{DMTS}}=I_{\mathrm{t/r}}P_{\mathrm{tx}}/P_{\mathrm{e}}(0\to 1)$ and $P_{\mathrm{e}}(0\to 1)\geqslant P_{\mathrm{e}}(\infty)=I_{\mathrm{t/r}}P_{\mathrm{tx}}/G_{\mathrm{SMTS}}$. Then, we have $G_{\mathrm{DMTS}}\leqslant G_{\mathrm{SMTS}}$, i.e., DMTS cannot provide a higher SIC performance than SMTS. To summarize,

Proposition 4. $G_{\mathrm{CMTS}}\geqslant G_{\mathrm{SMTS}}\geqslant G_{\mathrm{DMTS}}$, i.e., G_{CMTS} and G_{DMTS} are the upper and lower bounds of G_{SMTS}.

4 Power dissipation

Power dissipation of SMTS is caused as the N adjusted replicas of the transmit signal, i.e., $x_1, x_2, \ldots, x_N$, are summed up in the reconfigurable power combiner array. If the power dissipation of SMTS is too large, large power waste is caused and then the energy efficiency of SMTS is degraded significantly. To analyze this phenomenon quantitatively, this section defines a novel metric, called reconstruction power efficiency, to measure the power dissipation of SMTS. Based on the analysis of the power dissipation of SMTS, a method to minimize the power dissipation of SMTS is developed.

4.1 Reconstruction power efficiency

This subsection derives the reconstruction power efficiency of SMTS. The reconstruction power efficiency of a generalized multi-tap SIC circuit is defined as the ratio of the power of the reconstructed SI in this multi-tap SIC circuit to the power sum of all adjusted replicas of the transmit signal in this multi-tap SIC circuit, expressed as

$$\eta=\frac{\mathrm{E}\{\|\hat{r}_{\mathrm{si}}(t)\|^2\}}{\sum_{i=1}^{N}\mathrm{E}\{\|2^{\lceil\log_2(N)\rceil/2}a_i\mathrm{Re}\{b(t-\tau_i)\exp(\mathrm{j}\omega_c(t-\tau_i)+\mathrm{j}\phi_i)\}\|^2\}}=\frac{\boldsymbol{A}^{\mathrm{H}}\boldsymbol{O}^{\mathrm{H}}\boldsymbol{R}_b\boldsymbol{O}\boldsymbol{A}}{2^{\lceil\log_2(N)\rceil}\boldsymbol{A}^{\mathrm{H}}\boldsymbol{A}},\tag{13}$$

where $2^{\lceil\log_2(N)\rceil/2}$ is the additional scale adopted to compensate the insertion loss of the reconfigurable power combiner array, referring Proposition 1. It is observed from (13) that the insertion loss of the reconfigurable power combiner array degrades η significantly. In the definition of reconstruction power efficiency given by (13), the power dissipation caused by the insertion loss of the rat-race couplers in the reconfigurable power combiner array is omitted. With the property of the Rayleigh quotient [20], the variation range of η in (13) is derived as

$$\begin{aligned}\eta&\in\left[\lambda_{\min}\{\boldsymbol{O}^{\mathrm{H}}\boldsymbol{R}_b\boldsymbol{O}\}/2^{\lceil\log_2(N)\rceil},\lambda_{\max}\{\boldsymbol{O}^{\mathrm{H}}\boldsymbol{R}_b\boldsymbol{O}\}/2^{\lceil\log_2(N)\rceil}\right]\\&=\left[\lambda_{\min}\{\boldsymbol{R}_b\}/2^{\lceil\log_2(N)\rceil},\lambda_{\max}\{\boldsymbol{R}_b\}/2^{\lceil\log_2(N)\rceil}\right].\end{aligned}\tag{14}$$

To achieve significant SI reduction, the reconstructed SI $\hat{r}_{\mathrm{si}}(t)$ must have the similar power as the incoming SI $r_{\mathrm{si}}(t)$. Then, the power dissipation of a generalized multi-tap SIC structure approximates to $P_{\mathrm{tx}}I_{\mathrm{t/r}}/\eta$, which may be far larger than P_{tx} if the lower bound of η is far smaller than $I_{\mathrm{t/r}}$. In practice, the lower bound of η may be close to zero if $\boldsymbol{R}_b$ is close to singular, which will be caused as the number of taps is large and the delay lines in taps have too small delay interval. Thus, we have

Proposition 5. To avoid excessively high power dissipation in multi-tap SIC structure, the utilization of massive taps arranged with small delay must be avoid.

In SMTS, after G_{SMTS} is maximized, the reconstruction power efficiency of SMTS is computed by substituting $\boldsymbol{A}_{\mathrm{SMTS}}$ into (13) and given as

$$\eta_{\mathrm{SMTS}}=\frac{\mathrm{Re}\{\boldsymbol{O}^{\mathrm{H}}\boldsymbol{C}_b\boldsymbol{Q}\boldsymbol{H}\exp(-\mathrm{j}\phi_\infty)\}^{\mathrm{T}}\mathrm{Re}\{\boldsymbol{O}^{\mathrm{H}}\boldsymbol{R}_b\boldsymbol{O}\}^{-1}\mathrm{Re}\{\boldsymbol{O}^{\mathrm{H}}\boldsymbol{C}_b\boldsymbol{Q}\boldsymbol{H}\exp(-\mathrm{j}\phi_\infty)\}}{2^{\lceil\log_2(N)\rceil}\mathrm{Re}\{\boldsymbol{O}^{\mathrm{H}}\boldsymbol{C}_b\boldsymbol{Q}\boldsymbol{H}\exp(-\mathrm{j}\phi_\infty)\}^{\mathrm{T}}\mathrm{Re}\{\boldsymbol{O}^{\mathrm{H}}\boldsymbol{R}_b\boldsymbol{O}\}^{-2}\mathrm{Re}\{\boldsymbol{O}^{\mathrm{H}}\boldsymbol{C}_b\boldsymbol{Q}\boldsymbol{H}\exp(-\mathrm{j}\phi_\infty)\}},\tag{15}$$

which shows the dependence of η_{SMTS} on the SI channel $\boldsymbol{H}$. As the SI channel $\boldsymbol{H}$ varies, η_{SMTS} varies in $\eta_{\mathrm{SMTS}}\in\big[\lambda_{\min}\{\mathrm{Re}\{\boldsymbol{O}^{\mathrm{H}}\boldsymbol{R}_b\boldsymbol{O}\}\}/2^{\lceil\log_2(N)\rceil},\lambda_{\max}\{\mathrm{Re}\{\boldsymbol{O}^{\mathrm{H}}\boldsymbol{R}_b\boldsymbol{O}\}\}/2^{\lceil\log_2(N)\rceil}\big]$, which can be derived from (15) with the property of the Rayleigh quotient [20]. Since η_{SMTS} is located also in the range shown in (14), the variation range of η_{SMTS} is rewritten as

$$\begin{aligned}\eta_{\mathrm{SMTS}}\in\big[&\max(\lambda_{\min}\{\mathrm{Re}\{\boldsymbol{O}^{\mathrm{H}}\boldsymbol{R}_b\boldsymbol{O}\}\},\lambda_{\min}\{\boldsymbol{R}_b\})/2^{\lceil\log_2(N)\rceil},\\&\min(\lambda_{\max}\{\mathrm{Re}\{\boldsymbol{O}^{\mathrm{H}}\boldsymbol{R}_b\boldsymbol{O}\}\},\lambda_{\max}\{\boldsymbol{R}_b\})/2^{\lceil\log_2(N)\rceil}\big],\end{aligned}\tag{16}$$

which shows the dependency of η_{SMTS} on $\boldsymbol{R}_b$. Comparing η_{SMTS} with η_{CMTS} and η_{DMTS} derived in Appendix C yields

Proposition 6. The lower bounds of η_{DMTS} and η_{SMTS} are no smaller than the lower bound of η_{CMTS}, i.e., CMTS potentially has lower reconstruction power efficiency than DMTS and SMTS.

4.2 Maximization of the lower bound of η_{SMTS}

To avoid potential low reconstruction power efficiency of SMTS, the lower bound of η_{SMTS} has to be maximized, which is equivalent to maximizing $\lambda_{\min}\{\boldsymbol{R}_b\}$ and $\lambda_{\min}\{\mathrm{Re}\{\boldsymbol{O}^{\mathrm{H}}\boldsymbol{R}_b\boldsymbol{O}\}\}$. Since the sum of a matrix's eigenvalues is equal to its trace [21] and the traces of $\boldsymbol{R}_b$ and $\mathrm{Re}\{\boldsymbol{O}^{\mathrm{H}}\boldsymbol{R}_b\boldsymbol{O}\}$ are equal to N, $0\leqslant\lambda_{\min}\{\boldsymbol{R}_b\}\leqslant 1$, $0\leqslant\lambda_{\min}\{\mathrm{Re}\{\boldsymbol{O}^{\mathrm{H}}\boldsymbol{R}_b\boldsymbol{O}\}\}\leqslant 1$, $1\leqslant\lambda_{\max}\{\boldsymbol{R}_b\}\leqslant N$, and $1\leqslant\lambda_{\min}\{\mathrm{Re}\{\boldsymbol{O}^{\mathrm{H}}\boldsymbol{R}_b\boldsymbol{O}\}\}\leqslant N$ are satisfied, where $\boldsymbol{R}_b$ and $\mathrm{Re}\{\boldsymbol{O}^{\mathrm{H}}\boldsymbol{R}_b\boldsymbol{O}\}$ are positive semidefinite matrixes and thus have nonnegative eigenvalues. The upper bounds of $\lambda_{\min}\{\boldsymbol{R}_b\}$ and $\lambda_{\min}\{\mathrm{Re}\{\boldsymbol{O}^{\mathrm{H}}\boldsymbol{R}_b\boldsymbol{O}\}\}$ are equal to 1. To satisfy $\lambda_{\min}\{\boldsymbol{R}_b\}=1$ or $\lambda_{\min}\{\mathrm{Re}\{\boldsymbol{O}^{\mathrm{H}}\boldsymbol{R}_b\boldsymbol{O}\}\}=1$, all the eigenvalues of $\boldsymbol{R}_b$ or $\mathrm{Re}\{\boldsymbol{O}^{\mathrm{H}}\boldsymbol{R}_b\boldsymbol{O}\}$ must be equal to 1, which is equivalent to satisfying $\boldsymbol{R}_b=\boldsymbol{I}$ or $\mathrm{Re}\{\boldsymbol{O}^{\mathrm{H}}\boldsymbol{R}_b\boldsymbol{O}\}=\boldsymbol{I}$. Since $\mathrm{Re}\{\boldsymbol{O}^{\mathrm{H}}\boldsymbol{R}_b\boldsymbol{O}\}=\boldsymbol{I}$ is a necessary condition for $\boldsymbol{R}_b=\boldsymbol{I}$, satisfying $\boldsymbol{R}_b=\boldsymbol{I}$ or $\mathrm{Re}\{\boldsymbol{O}^{\mathrm{H}}\boldsymbol{R}_b\boldsymbol{O}\}=\boldsymbol{I}$ is equivalent to satisfying $\mathrm{Re}\{\boldsymbol{O}^{\mathrm{H}}\boldsymbol{R}_b\boldsymbol{O}\}=\boldsymbol{I}$. Thus, we have

Proposition 7. Maximization of the lower bound of η_{SMTS} is equivalent to satisfying $\mathrm{Re}\{\boldsymbol{O}^{\mathrm{H}}\boldsymbol{R}_b\boldsymbol{O}\}=\boldsymbol{I}$, which means that the input signals of the N taps are uncorrelated with one another.

5 Simulations

This section performs simulations to illustrate the SIC performance and power dissipation of the proposed SMTS. For comparisons, CMTS and DMTS are also simulated. In the simulations, the delay lines in taps are built by following $\tau_k=\Delta\tau(k-1)$ ns, where $k=1,2,\ldots,N$ is the tap index and $\Delta\tau$ is the delay interval. The 64-ray quadrature amplitude modulation and the root-raised cosine pulse shape filter with roll-off factor of 0.22 are adopted to generate the transmit signal. The transmit signal is centered at 2.4 GHz with a power of 0 dBm. Moreover, the noise floor at the receiver frontend is -174 dBm/Hz. This section is arranged as follows. First, the SI channel is modeled according to the published measurement results of FD prototypes. Next, the numerical algorithm developed for the computation of SIC performance provided by SMTS is simulated to illustrate its convergence with the increment of the iteration time. Then, the SIC performance provided by SMTS is simulated and discussed. After that, the impact of the multi-tap SIC circuit on the coupling channel between transmitter and receiver is illustrated. Finally, the power dissipation of SMTS is simulated and discussed.

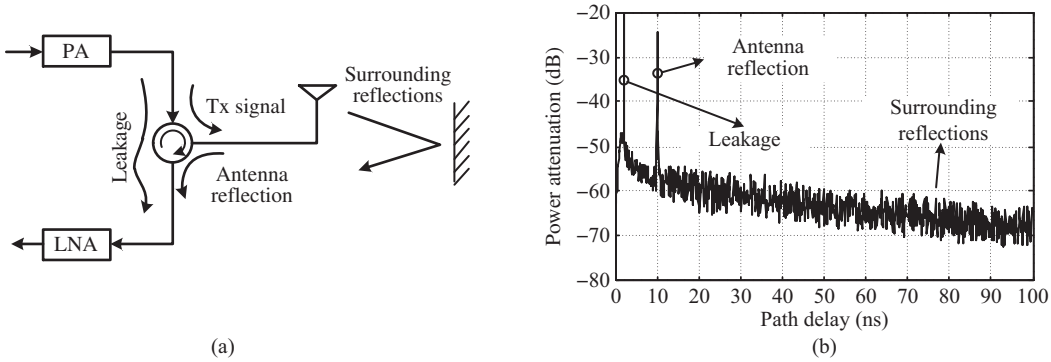

Figure 4 (a) Considered FD transceiver frontend; (b) power delay profile of SI channel.

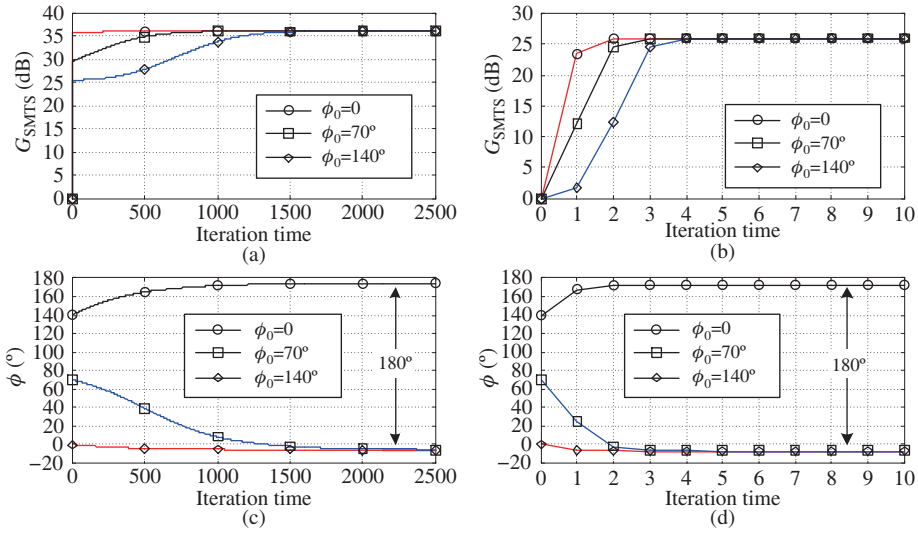

Figure 5 (Color online) Convergence of the developed numerical algorithm with 7 taps, i.e., $N = 7$. (a) G_{SMTS} vs. iteration time for 20-MHz SI; (b) G_{SMTS} vs. iteration time for 100-MHz SI; (c) ϕ vs. iteration time for 20-MHz SI; (d) ϕ vs. iteration time for 100-MHz SI.

5.1 SI channel

The adopted SI channel in the simulations is modeled in this subsection. The considered FD radio frontend is shown in Figure 4(a), where the transmitter and the receiver share one antenna through a circulator. The SI channel in this FD radio is modeled according to the measurement results in [14] with a time resolution of up to 0.1 ns to emulate the realistic time-continuous channel as much as possible. The magnitude profile of the paths of the SI channel is shown in Figure 4(b), where the two peaks are the circulator leakage and the antenna reflection, respectively, and the rests are random reflections caused by surroundings. The phase shifts of the paths of the SI channel are uniformly distributed on $[-\pi, \pi)$ [17].

5.2 Convergence of the developed numerical algorithm

This subsection performs simulations to verify the convergence of the developed numerical algorithm and plots the simulation results in Figure 5, where the power of the residual SI is converted to the SIC performance with (11) for clarity. In the simulations, $\varphi_1, \varphi_2, \ldots, \varphi_M$ are configured with 0 while the shared phase shifter is configured with different initial values. It is clear that objectives converge as the iteration time increases in all simulations. Configuring the shared phase shifter with different initial values, G_{SMTS} converges with different convergence speed to the same limit value. In Figure 5 (c) and (d), the limit values of ϕ have a difference of 180 degrees, which is caused by the inversion of the scales.

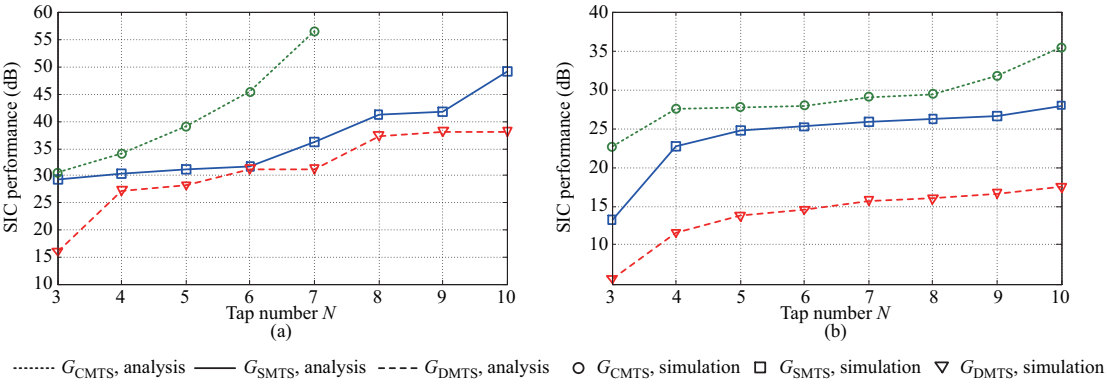

Figure 6 (Color online) SIC performance vs. tap number. (a) 20-MHz SI; (b) 100-MHz SI.

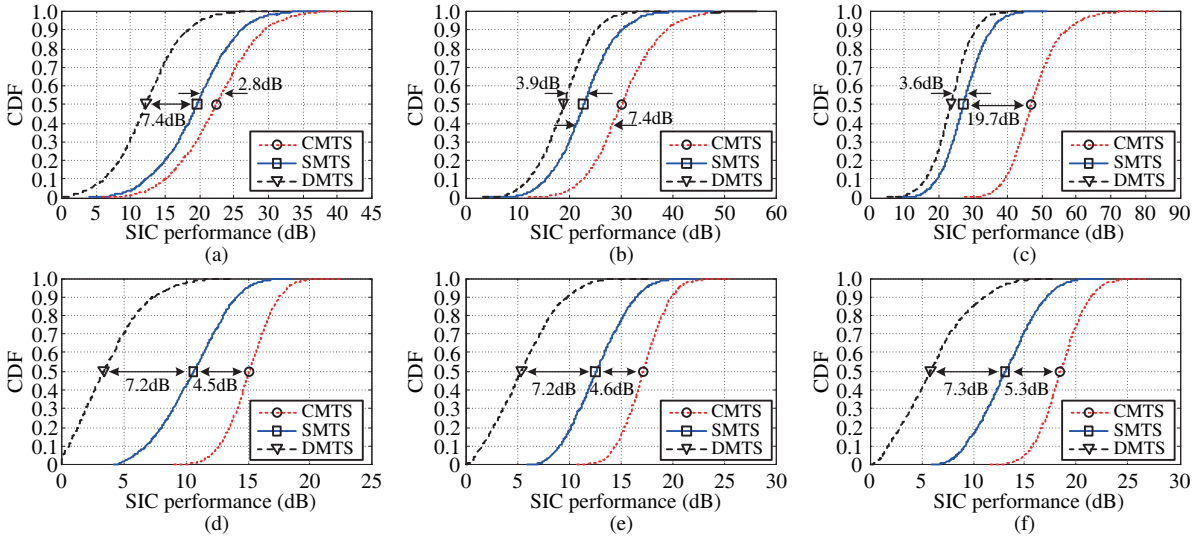

Figure 7 (Color online) CDF of SIC performance. (a) 20-MHz SI and $N = 3$; (b) 20-MHz SI and $N = 5$; (c) 20-MHz SI and $N = 7$; (d) 100-MHz SI and $N = 3$; (e) 100-MHz SI and $N = 5$; (f) 100-MHz SI and $N = 7$. Simulations are performed by 3000 times.

5.3 SIC performance

This subsection performs simulations to illustrate impacts of the number of taps and the SI channel on the SIC performance provided by SMTS. In the simulations, the delay interval is configured with $\Delta\tau = 4$ ns, $\varphi_1, \varphi_2, \ldots, \varphi_M$ are configured with 0, and the SI channel provides a SI reduction of about 19 dB. The variation of the SIC performance provided by SMTS with the increment of the number of taps is plotted in Figure 6. It is observed from all curves in Figure 6 that the results obtained from the analysis exhibit an accurate fit with the simulations and the increment of the number of taps always improves the SIC performance. Nevertheless, the improvement of SIC performance caused by the increment of the number of taps may be negligible in SMTS and DMTS. For instance, in Figure 6(a), G_{SMTS} is improved by no more than 1 dB as N increases from 5 to 6 and G_{DMTS} is improved by no more than 0.5 dB as N increases from 6 to 7. In addition, the SIC performance provided by SMTS is close to CMTS in case of the 100-MHz SI. That means SMTS is more suitable for the cancellation of broadband SI than the cancellation of narrowband SI. Besides, the results verifies the discussions in Proposition 4.

The impact of the SI channel on the SIC performance provided by SMTS is simulated and the simulation results are plotted in form of cumulative distribution function (CDF) in Figure 7. In the simulations, $\varphi_1, \varphi_2, \ldots, \varphi_M$ are independently and uniformly distributed on $[-\pi, \pi)$. The simulation results show that CMTS, DMTS, and SMTS all can provide SIC performance. In Figure 7 (a) and (d)–(f), the SIC performance provided by SMTS is significantly higher than the SIC performance provided by DMTS and

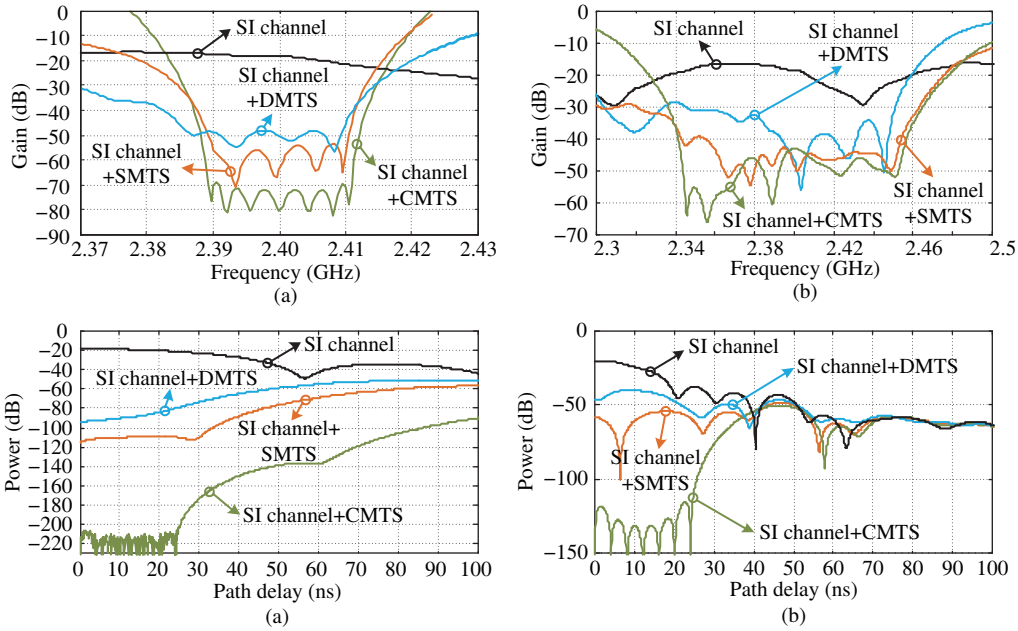

Figure 8 (Color online) Coupling channel. The tap number is 7, i.e., $N = 7$. (a) Magnitude response with 20-MHz SI; (b) magnitude response with 100-MHz SI; (c) time domain response with 20-MHz SI; (d) time domain response with 100-MHz SI.

close to the SIC performance provided by CMTS. In Figure 7 (b) and (c), CMTS provides significantly high the SIC performance due to the increment of the number of taps, from which SMTS benefits much less. Besides, CMTS, DMTS, and SMTS all provide lower SIC performance over larger bandwidth, and thus cancelling the broadband SI is a challenging problem for multi-tap analog SIC. In all subfigures of Figure 7, the simulation results scatter in a relatively large range of SIC performance. That means the SIC performances provided by CMTS, SMTS and DMTS have high sensitivity to the variation of SI channel. It's worth noting that the CDF curves of the SIC performance provided by DMTS in Figure 7 (d)–(f) reach to the SIC performance of 0 dB. That means DMTS may not provide any reduction of broadband SI, and thus is not suitable for the cancellation of broadband SI.

5.4 Coupling channel

In a FD radio, the coupling channel between transmitter and receiver is the combination of the SI channel and the adopted SIC circuit. This subsection performs simulations to illustrate the the coupling channel in forms of frequency domain response and time domain response, and plots the simulation results in Figure 8. In the simulations, 7 taps are adopted and the delay lines are arranged with a delay interval $\Delta\tau = 4$ ns to cover a delay range from 0 to 24 ns. In Figure 8 (a) and (b), the SI channel provides low attenuation over the operating band, and thus leads to strong SI at the receiver. In existence of CMTS, DMTS, or SMTS, the attenuation of the coupling channel over the operating band is improved significantly. It is visualized that CMTS, SMTS, and DMTS provide the highest, the medium, and the lowest improvements of attenuation over the operating band, respectively. It is worth noting that the coupling channel becomes more frequency selective in existence of CMTS, SMTS, and DMTS, and thus the following SIC stage, such as the frequently-used digital SIC stage, has to consider the incoming SI as a multipath signal.

In Figure 8 (c) and (d), the power level of the time domain response of the coupling channel is degraded more significantly in the coverage of the delay lines than out of the coverage of the delay lines. In other words, the paths of the SI channel out of the coverage of the delay lines is difficult to be canceled. However, the large-delayed strong paths which can saturate the receiver must be canceled at the front of the receiver. Considering the delay line which provides large delay is difficult to manufacture at present, cancelling the large-delayed strong paths is a challenging problem for multi-tap analog SIC.

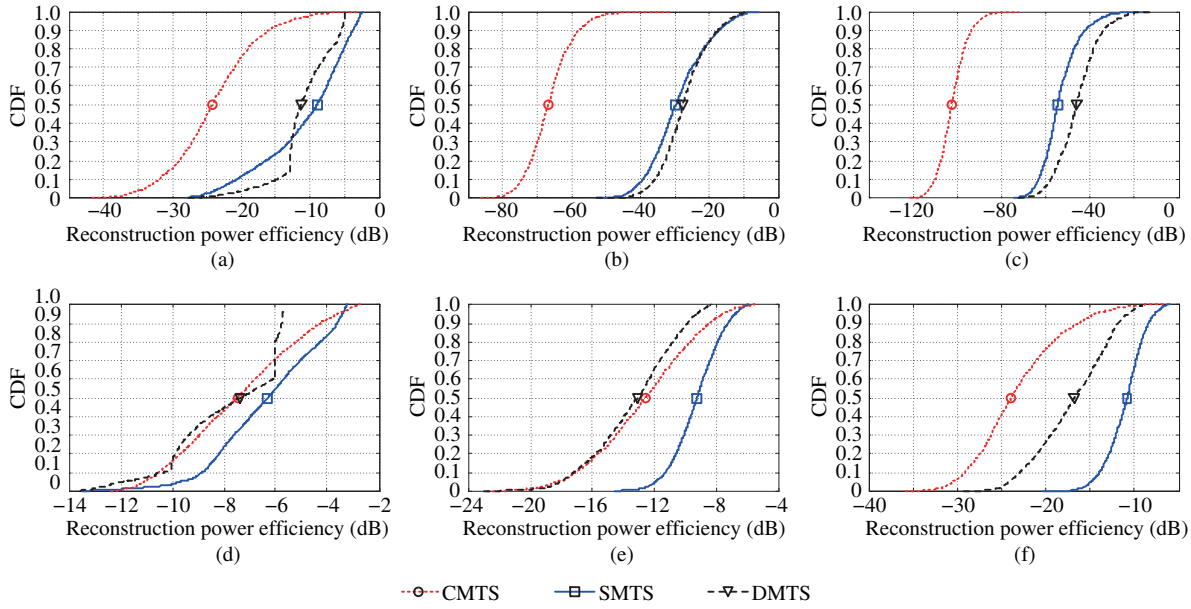

Figure 9 (Color online) CDF of reconstruction power efficiency. The delay interval of the delay lines is $\Delta\tau = 4$ ns. (a) 20-MHz SI and $N = 3$; (b) 20-MHz SI and $N = 5$; (c) 20-MHz SI and $N = 7$; (d) 100-MHz SI and $N = 3$; (e) 100-MHz SI and $N = 5$; (f) 100-MHz SI and $N = 7$. Simulations are performed by 3000 times.

Table 3 Comparisons of CMTS, DMTS, and SMTS with N taps

Item	CMTS	DMTS	SMTS
1. SIC performance	Highest	Lowest	Medium
2. Quantity of variable phase shifters	N	0	1
3. Quantity of power combiners[a)]	$2^{\lceil \log_2(N) \rceil} - 1$	$2^{\lceil \log_2(N) \rceil} - 1$	$2^{\lceil \log_2(N) \rceil} - 1$
4. Quantity of selectors	0	0	$2^{\lceil \log_2(N) \rceil} - 1$
5. Reconstruction power efficiency	Lowest	Medium	Highest
6. Dimensions of control algorithm	$2N$	N	$N + 1$

a) Here suppose that the power combiner arrays in CMTS and DMTS are also tree structure.

5.5 Power dissipation

This section performs simulations to illustrate the power dissipation of SMTS and the simulation results are plotted in Figure 9, where $\varphi_1, \varphi_2, \ldots, \varphi_M$ are independently and uniformly distributed on $[-\pi, \pi)$. The simulation results show that the reconstruction power efficiency of SMTS decreases as the number of taps increases. Furthermore, the reconstruction power efficiency of SMTS is far larger in case of 100-MHz SI than in case of 20-MHz SI. That means the reconstruction power efficiency is sensitive to the bandwidth of SI. Moreover, CMTS leads to much lower reconstruction power efficiency than DMTS and SMTS, which verifies Proposition 6. In Figure 9 (b) and (c), CMTS, DMTS, and SMTS all have excessively low reconstruction power efficiency, which means excessively high power dissipation in implementations and verifies Proposition 5. In Figure 9 (a) and (d)–(f) where the reconstruction power efficiencies of CMTS, DMTS, and SMTS are moderate, SMTS has the highest reconstruction power efficiency.

6 Conclusion

This paper proposes a novel SIC structure, called SMTS, for FD communications. The proposed architecture adopts one shared phase shifter to emulate the dominated phase offset of the SI channel to achieve high SIC performance as well as low implementation complexity. The comparisons between the proposed architecture and the existing architectures, summarized in Table 3, show that the proposed ar-

chitecture adopts the medium quantity of the variable analog devices to provide the close-to-optimal SIC performance at the cost of the highest reconstruction power efficiency. Relative to CMTS and DMTS, the proposed architecture does not have significant drawbacks, and thus is more suitable for FD applications.

Acknowledgements This work was supported by National Natural Science Foundation of China (Grant Nos. 61531009, 61501093, 61271164, 61471108) and Fundamental Research Funds for the Central Universities.

Conflict of interest The authors declare that they have no conflict of interest.

References

1 Zhang Z S, Long K P, Vasilakos A V, et al. Full-duplex wireless communications: challenges, solutions, and future research directions. Proc IEEE, 2016, 104: 1369–1409
2 Ma Z, Zhang Z Q, Ding Z G, et al. Key techniques for 5G wireless communications: network architecture, physical layer, and MAC layer perspectives. Sci China Inf Sci, 2015, 58: 041301
3 Lu H T, Shao S H, Deng K, et al. Self-mixed self-interference analog cancellation in full-duplex communications. Sci China Inf Sci, 2016, 59: 042303
4 Zhang G P, Yang K, Liu P, et al. Using full duplex relaying in device-to-device (D2D) based wireless multicast services: a two-user case. Sci China Inf Sci, 2015, 58: 082301
5 Zhang Z L, Shen Y, Shao S H, et al. Full duplex 2×2 MIMO radios. In: Proceedings of International Conference on Wireless Communications and Signal Processing (WCSP'14), Hefei, 2014. 1–6
6 Kolodziej K E, McMichael J G, Perry B T. Adaptive RF canceller for transmit-receive isolation improvement. In: Proceedings of IEEE Radio and Wireless Symposium (RWS'14), Newport Beach, 2014. 172–174
7 Chen T Y, Liu S. A multi-stage self-interference canceller for full-duplex wireless communications. In: Proceedings of IEEE Global Communications Conference (GLOBECOM'15), San Diego, 2015. 1–6
8 Kolodziej K E, McMichael J G, Perry B T. Multi-tap RF canceller for in-band full-duplex wireless communications. IEEE Trans Wirel Commun, 2016, 15: 4321–4334
9 Choi J, Jain M, Srinivasan K, et al. Achieving single channel, full duplex wireless communication. In: Proceedings of the 16th Annual International Conference on Mobile Computing and Networking (MobiCom'10), Chicago, 2010. 1–12
10 Jain M, Choi J I, Kim T, et al. Practical, real-time, full duplex wireless. In: Proceedings of the 17th Annual International Conference on Mobile Computing and Networking (MobiCom'11), Las Vegas, 2011. 301–312
11 Bharadia D, Mcmilin E, Katti S. Full duplex radios. In: Proceedings of the ACM SIGCOMM 2013 Conference (SIGCOMM'13), Hong Kong, 2013. 375–386
12 Bharadia D, Katti S. Full duplex MIMO radios. In: Proceedings of the 11th USENIX Conference on Networked Systems Design and Implementation (NSDI'14), Seattle, 2014. 359–372
13 Mayer U, Wickert M, Eickhoff R, et al. 2-6-GHz BiCMOS polar-based vector modulator for S- and C-band diversity receivers. IEEE Trans Microw Theory Tech, 2012, 60: 567–573
14 Wu X Y. The measurement and analysis of the co-time co-frequency full-duplex self-interference channel. Dissertation for the Doctoral Degree. Chengdu: University of Electronic Science and Technology of China, 2015. 40–41, 66–67
15 Sahai A, Patel G, Dick C, et al. On the impact of phase noise on active cancelation in wireless full-duplex. IEEE Trans Veh Technol, 2013, 62: 4494–4510
16 Hua Y B, Ma Y M, Gholian A, et al. Radio self-interference cancellation by transmit beamforming, all-analog cancellation and blind digital tuning. Signal Process, 2015, 108: 322–340
17 Goldsmith A. Wireless Communications. New York: Cambridge University Press, 2005. 26–27
18 Xu H X, Wang G M, Lu K. Microstrip rat-race couplers. IEEE Microw Mag, 2011, 12: 117–129
19 Boyd S, Vandenberghe L. Convex Optimization. Cambridge: Cambridge University Press, 2004. 457–520, 153–154
20 Gradshteyn I S, Ryzhik I M. Table of Integrals, Series, and Products. 7th ed. CA: Scripta Technica, 2007. 1081–1091
21 Petersen K B, Pedersen M S. The Matrix Cookbook. Massachusetts Institute of Technology (MIT) Tech Rep. 2012

Appendix A SIC performance provided by CMTS

Replacing $\boldsymbol{A}$ in (5) by $\boldsymbol{A}_{\mathrm{CMTS}} = [a_1 \exp(\mathrm{j}\phi_1) a_2 \exp(\mathrm{j}\phi_2) \cdots \ a_N \exp(\mathrm{j}\phi_N)]^{\mathrm{T}}$ yields the power of residual SI of CMTS $P_{\mathrm{e,CMTS}}$, where $\phi_1, \phi_2, \ldots, \phi_N$ are the phase offsets of the N variable phase shifters in CMTS. The optimal $\boldsymbol{A}_{\mathrm{CMTS}}$ to minimize $P_{\mathrm{e,CMTS}}$ is an unconstrained minimization problem and can be solved by ordering $0 = \nabla P_{\mathrm{e,CMTS}}$ [19], i.e.,

$$\begin{cases} 0 = \partial P_{\mathrm{e,CMTS}}/\partial \mathrm{Re}\{\boldsymbol{A}_{\mathrm{CMTS}}\} = -2\mathrm{Re}\{\boldsymbol{O}^{\mathrm{H}}\boldsymbol{C}_b\boldsymbol{Q}\boldsymbol{H}\} + 2\mathrm{Re}\{\boldsymbol{O}^{\mathrm{H}}\boldsymbol{R}_b\boldsymbol{O}\}\mathrm{Re}\{\boldsymbol{A}_{\mathrm{CMTS}}\} - 2\mathrm{Im}\{\boldsymbol{O}^{\mathrm{H}}\boldsymbol{R}_b\boldsymbol{O}\}\mathrm{Im}\{\boldsymbol{A}_{\mathrm{CMTS}}\}, \\ 0 = \partial P_{\mathrm{e,CMTS}}/\partial \mathrm{Im}\{\boldsymbol{A}_{\mathrm{CMTS}}\} = -2\mathrm{Im}\{\boldsymbol{O}^{\mathrm{H}}\boldsymbol{C}_b\boldsymbol{Q}\boldsymbol{H}\} + 2\mathrm{Re}\{\boldsymbol{O}^{\mathrm{H}}\boldsymbol{R}_b\boldsymbol{O}\}\mathrm{Im}\{\boldsymbol{A}_{\mathrm{CMTS}}\} + 2\mathrm{Im}\{\boldsymbol{O}^{\mathrm{H}}\boldsymbol{R}_b\boldsymbol{O}\}\mathrm{Re}\{\boldsymbol{A}_{\mathrm{CMTS}}\}. \end{cases} \tag{A1}$$

The solution of (A1) is derived as $\boldsymbol{A}_{\mathrm{CMTS}} = \boldsymbol{O}^{-1}\boldsymbol{R}_b^{-1}\boldsymbol{C}_b\boldsymbol{Q}\boldsymbol{H}$, which is the well-known Wiener solution[3)]. Then the SIC performance provided by CMTS is computed with (11) and given as

$$G_{\mathrm{CMTS}} = I_{\mathrm{t/r}}(I_{\mathrm{t/r}} - \boldsymbol{H}^{\mathrm{H}}\boldsymbol{Q}^{\mathrm{H}}\boldsymbol{C}_b^{\mathrm{H}}\boldsymbol{R}_b^{-1}\boldsymbol{C}_b\boldsymbol{Q}\boldsymbol{H})^{-1}. \tag{A2}$$

3) Diniz P S R. Adaptive filtering—algorithms and practical implementation. 3rd ed. Spring Street, NY: Springer Science & Business Media, 2008. 25–47.

Appendix B SIC performance provided by DMTS

In DMTS, the power of residual SI $P_{\mathrm{e,DMTS}}$ is obtained by replacing $\boldsymbol{A}$ by $\tilde{\boldsymbol{A}}$ in (5). Finding the optimal tap coefficients in DMTS to minimize $P_{\mathrm{e,DMTS}}$ is expressed as

$$\begin{aligned}&\min\ P_{\mathrm{e,DMTS}}\\ &\text{subject to } \tilde{\boldsymbol{A}}\geqslant 0\end{aligned}\ \Leftrightarrow\ \begin{aligned}&\min\ \left\|\begin{bmatrix}\mathrm{Re}(\boldsymbol{\Lambda}^{1/2}\boldsymbol{U}^{-1}\boldsymbol{O})\\ \mathrm{Im}(\boldsymbol{\Lambda}^{1/2}\boldsymbol{U}^{-1}\boldsymbol{O})\end{bmatrix}\tilde{\boldsymbol{A}}-\begin{bmatrix}\mathrm{Re}(\boldsymbol{\Lambda}^{-1/2}\boldsymbol{U}^{-1}\boldsymbol{C}_b\boldsymbol{Q}\boldsymbol{H})\\ \mathrm{Im}(\boldsymbol{\Lambda}^{-1/2}\boldsymbol{U}^{-1}\boldsymbol{C}_b\boldsymbol{Q}\boldsymbol{H})\end{bmatrix}\right\|_2^2,\\ &\text{subject to } \tilde{\boldsymbol{A}}\geqslant 0\end{aligned}\tag{B1}$$

where $\boldsymbol{R}_b=\boldsymbol{U}\boldsymbol{\Lambda}\boldsymbol{U}^{\mathrm{H}}$[2)], $\boldsymbol{\Lambda}$ is the diagonal matrix consisting of the eigenvalues of $\boldsymbol{R}_b$, $\boldsymbol{U}$ is the unitary matrix consisting of the normalized eigenvectors of $\boldsymbol{R}_b$, and $\|\cdot\|_2$ is the Euclidean norm of a vector [20]. Eq. (B1) is an nonnegative least squares optimization problem and can be solved with various well-developed numerical approaches[4)], and then the SIC performance provided by DMTS is computed with (11) and given as

$$G_{\mathrm{DMTS}}=I_{\mathrm{t/r}}(I_{\mathrm{t/r}}-2\mathrm{Re}\{\boldsymbol{H}^{\mathrm{H}}\boldsymbol{Q}^{\mathrm{H}}\boldsymbol{C}_b^{\mathrm{H}}\boldsymbol{O}\}\boldsymbol{A}_{\mathrm{DMTS}}+\boldsymbol{A}_{\mathrm{DMTS}}^{\mathrm{T}}\mathrm{Re}\{\boldsymbol{O}^{\mathrm{H}}\boldsymbol{R}_b\boldsymbol{O}\}\boldsymbol{A}_{\mathrm{DMTS}})^{-1},\tag{B2}$$

where $\boldsymbol{A}_{\mathrm{DMTS}}$ is the numerical result of (B1).

The upper bound of G_{DMTS} is derived as follows. Relaxing the constraint $\tilde{\boldsymbol{A}}\geqslant 0$, the optimal $\tilde{\boldsymbol{A}}$ for (B1) is derived as $\hat{\boldsymbol{A}}_{\mathrm{DMTS}}=\mathrm{Re}\{\boldsymbol{O}^{\mathrm{H}}\boldsymbol{R}_b\boldsymbol{O}\}^{-1}\mathrm{Re}\{\boldsymbol{O}^{\mathrm{H}}\boldsymbol{C}_b\boldsymbol{Q}\boldsymbol{H}\}$ by ordering $0=\nabla P_{\mathrm{e,DMTS}}$ [19], and then the corresponding SIC performance is computed with (5) and (11) as $\hat{G}_{\mathrm{DMTS}}=I_{\mathrm{t/r}}(I_{\mathrm{t/r}}-\mathrm{Re}\{\boldsymbol{O}^{\mathrm{H}}\boldsymbol{C}_b\boldsymbol{Q}\boldsymbol{H}\}^{\mathrm{T}}\mathrm{Re}\{\boldsymbol{O}^{\mathrm{H}}\boldsymbol{R}_b\boldsymbol{O}\}^{-1}\mathrm{Re}\{\boldsymbol{O}^{\mathrm{H}}\boldsymbol{C}_b\boldsymbol{Q}\boldsymbol{H}\})^{-1}$. To compare $\hat{G}_{\mathrm{DMTS}}$ with G_{DMTS}, $1/G_{\mathrm{DMTS}}-1/\hat{G}_{\mathrm{DMTS}}=\|\boldsymbol{\Sigma}^{-1/2}\boldsymbol{V}^{\mathrm{H}}\mathrm{Re}\{\boldsymbol{O}^{\mathrm{H}}\boldsymbol{C}_b\boldsymbol{Q}\boldsymbol{H}\}-\boldsymbol{\Sigma}^{1/2}\boldsymbol{V}^{\mathrm{H}}\boldsymbol{A}_{\mathrm{DMTS}}\|_2^2/I_{\mathrm{t/r}}\geqslant 0$ is computed, and then $\hat{G}_{\mathrm{DMTS}}\geqslant G_{\mathrm{DMTS}}$ is derived, i.e., $\hat{G}_{\mathrm{DMTS}}$ is the upper bound of G_{DMTS}, where $\mathrm{Re}\{\boldsymbol{O}^{\mathrm{H}}\boldsymbol{R}_b\boldsymbol{O}\}=\boldsymbol{V}\boldsymbol{\Sigma}\boldsymbol{V}^{\mathrm{H}}$, $\boldsymbol{\Sigma}$ is the diagonal matrix consisting of the eigenvalues of $\mathrm{Re}\{\boldsymbol{O}^{\mathrm{H}}\boldsymbol{R}_b\boldsymbol{O}\}$, $\boldsymbol{V}$ is the unitary matrix consisting of the normalized eigenvectors of $\mathrm{Re}\{\boldsymbol{O}^{\mathrm{H}}\boldsymbol{R}_b\boldsymbol{O}\}$.

Appendix C Reconstruction power efficiencies of CMTS and DMTS

After G_{CMTS} and G_{DMTS} are maximized, the reconstruction power efficiencies of CMTS and DMTS are computed by substituting $\boldsymbol{A}_{\mathrm{CMTS}}$ and $\boldsymbol{A}_{\mathrm{DMTS}}$ into (13) and given as

$$\begin{cases}\eta_{\mathrm{CMTS}}=((\boldsymbol{C}_b\boldsymbol{Q}\boldsymbol{H})^{\mathrm{H}}\boldsymbol{R}_b^{-1}\boldsymbol{C}_b\boldsymbol{Q}\boldsymbol{H})/((\boldsymbol{C}_b\boldsymbol{Q}\boldsymbol{H})^{\mathrm{H}}\boldsymbol{R}_b^{-2}\boldsymbol{C}_b\boldsymbol{Q}\boldsymbol{H})/2^{\lceil\log_2(N)\rceil},\\ \eta_{\mathrm{DMTS}}=(\boldsymbol{A}_{\mathrm{DMTS}}^{\mathrm{T}}\mathrm{Re}\{\boldsymbol{O}^{\mathrm{H}}\boldsymbol{R}_b\boldsymbol{O}\}\boldsymbol{A}_{\mathrm{DMTS}})/(\boldsymbol{A}_{\mathrm{DMTS}}^{\mathrm{T}}\boldsymbol{A}_{\mathrm{DMTS}})/2^{\lceil\log_2(N)\rceil},\end{cases}\tag{C1}$$

respectively, where the fixed power combiner arrays in CMTS and DMTS are assumed to also have the tree structure, and thus likewise have an insertion loss $2^{\lceil\log_2(N)\rceil}$. With the property of the Rayleigh quotient [20], $\eta_{\mathrm{DMTS}}\in[\lambda_{\min}\{\mathrm{Re}\{\boldsymbol{O}^{\mathrm{H}}\boldsymbol{R}_b\boldsymbol{O}\}\}/2^{\lceil\log_2(N)\rceil},\lambda_{\max}\{\mathrm{Re}\{\boldsymbol{O}^{\mathrm{H}}\boldsymbol{R}_b\boldsymbol{O}\}\}/2^{\lceil\log_2(N)\rceil}]$ and $\eta_{\mathrm{CMTS}}\in[\lambda_{\min}\{\boldsymbol{R}_b\}/2^{\lceil\log_2(N)\rceil},\ \lambda_{\max}\{\boldsymbol{R}_b\}/2^{\lceil\log_2(N)\rceil}]$ can be derived from (C1). Combining with (14), the variation ranges of η_{CMTS} and η_{DMTS} are summarized as

$$\begin{cases}\eta_{\mathrm{CMTS}}\in[\lambda_{\min}\{\boldsymbol{R}_b\}/2^{\lceil\log_2(N)\rceil},\lambda_{\max}\{\boldsymbol{R}_b\}/2^{\lceil\log_2(N)\rceil}],\\ \eta_{\mathrm{DMTS}}\in[\max(\lambda_{\min}\{\mathrm{Re}\{\boldsymbol{O}^{\mathrm{H}}\boldsymbol{R}_b\boldsymbol{O}\}\},\lambda_{\min}\{\boldsymbol{R}_b\})/2^{\lceil\log_2(N)\rceil},\min(\lambda_{\max}\{\mathrm{Re}\{\boldsymbol{O}^{\mathrm{H}}\boldsymbol{R}_b\boldsymbol{O}\}\},\lambda_{\max}\{\boldsymbol{R}_b\})/2^{\lceil\log_2(N)\rceil}],\end{cases}\tag{C2}$$

respectively.

4) Chen D, Plemmons R. Nonnegativity constraints in numerical analysis. In: Bultheel A, Cools R, eds. The Birth of Numerical Analysis. Hackensack: World Scientific, 2010. 109–139.